UC Irvine
UC Irvine Previously Published Works

Title

Unpacking the diversity of monoterpene oxidation pathways via nitrooxy—alkyl radical ring-opening reactions and nitrooxy—alkoxyl radical bond scissions

Permalink

https://escholarship.org/uc/item/9b6848t6

Authors

Draper, Danielle
Almeida, Thomas Golin
Iyer, Siddharth
et al.

Publication Date

2024-06-01

DOI

10.1016/j.jaerosci.2024.106379

Peer reviewed

eScholarship.org Powered by the California Digital Library
University of California

Unpacking the diversity of monoterpene oxidation pathways via nitrooxy–alkyl radical ring-opening reactions and nitrooxy–alkoxyl radical bond scissions

Danielle Draper[a,*], Thomas Golin Almeida[b,c,*], Siddharth Iyer[d], James N. Smith[a], Theo Kurtén[b,c,**], Nanna Myllys[b,c,**]

[a]*Department of Chemistry, University of California, Irvine, USA*
[b]*Department of Chemistry, University of Helsinki, Helsinki 00014, Finland*
[c]*Institute for Atmospheric and Earth System Research, University of Helsinki, Helsinki 00014, Finland*
[d]*Aerosol Physics Laboratory, Tampere University, Tampere FI-3720, Finland*

Abstract

Terrestrial vegetation emits vast quantities of monoterpenes to the atmosphere. These compounds, once oxidized, can contribute to the formation and growth of secondary organic aerosol (SOA) particles. However, studies report widely different SOA yields from atmospheric oxidation of different monoterpenes, despite their structural similarities. The NO_3-radical-initiated oxidation of α-pinene for instance, leads to minimal SOA yields, whereas with Δ-carene a high SOA yield is observed. A previous study indicated that their oxidation mechanisms diverge after formation of a nitrooxy–alkoxyl radical intermediate, whose C−C bond scission reactions can either lead to early termination of the oxidative chain, thus limiting the yield of condensable vapors, or further propagate it, leading to low-volatility products. In this study, we employ computational methods to investigate these reactions in the NO_3-radical oxidation of five other monoterpenes: limonene, sabinene, β-pinene, α-thujene and camphene. Additionally, we explore the possibility of rearrangement via ring-opening of the nitrooxy-alkyl radical adducts produced immediately after NO_3 radical attack. Our calculations predict that

*Authors contributed equally
**Corresponding authors
Email addresses: theo.kurten@helsinki.fi (Theo Kurtén), nanna.myllys@helsinki.fi (Nanna Myllys)

alkyl radical rearrangement is dominant over O_2-addition for sabinene, minor but competitive for α-thujene and β-pinene, and negligible for camphene. These rearrangements can induce further propagation of the oxidative chain, and thus higher SOA yields. Concerning alkoxyl radical C−C bond scissions, our results indicate that endocyclic nitrate species (derived from limonene and α-thujene) react preferentially via the channel leading to oxidative chain termination, whereas exocyclic nitrate species (sabinene, β-pinene, and camphene) react preferentially via channels leading to further propagation.

Keywords: monoterpene, oxidation, nitrooxy–alkyl radical ring opening, nitrooxy–alkoxyl radical bond scissions

---

1. Introduction

Monoterpenes ($C_{10}H_{16}$) have long been studied as a significant contributor to secondary organic aerosol (SOA) formation and growth. They are estimated to contribute approximately 15% of global biogenic (non-methane) volatile organic compound (VOC) emissions, and due to their relatively low starting volatility, monoterpenes tend to have a high yield of condensable products once oxidized (Guenther et al., 2012). Field observations around the world have shown that a major fraction of organic aerosol (OA) is secondary in nature (Zhang et al., 2007), meaning that it forms from gas-phase chemical reactions (e.g. oxidation) of organic precursors, and individual field studies have been able to attribute substantial fractions of observed SOA to monoterpene-derived products specifically. For example, in the southeastern US it was estimated that monoterpene chemistry contributed to roughly half of the total observed OA (Zhang et al., 2018). While we know that aerosols in the atmosphere play an important role in the climate system by interacting with incoming solar radiation and seeding clouds, aerosols represent the largest source of uncertainty in estimates of radiative forcing in the atmosphere due to their complexity (Myhre et al., 2013). Many formation and aging processes as well as physicochemical properties are still poorly understood (Hallquist et al., 2009; Shrivastava et al., 2017; Bianchi et al., 2019). Further, small-sized particles (i.e. size ranges often dominated by formation and growth of SOA) can have adverse effects on human health upon inhalation due to their ability to permeate lung tissue and enter the bloodstream (Pope III & Dockery, 2006; Schraufnagel, 2020; Atkinson et al., 2015), which gives an additional layer of urgency to better understand SOA formation and growth processes. Due to their structural similarities, oxidation of different monoterpenes may proceed along quite similar mechanistic pathways. However, numerous studies have shown striking differences in SOA yields between different monoterpenes (Hallquist et al., 1999; Griffin et al., 1999; Fry et al., 2014; Ng et al., 2017), indicating that there must be impactful differences in their oxidation mechanisms.

Kurtén et al. (2017) investigated the detailed oxidation mechanisms for two chemical systems with one of the most extreme SOA yield disparities: the NO_3 radical oxidation of α-pinene and Δ-carene. These two bicyclic monoterpenes differ only by the size and placement of their secondary ring structure, and yet α-pinene has a negligible SOA yield from NO_3 oxidation, while Δ-carene has observed SOA yields ranging from 12–74% (Ng et al.,

2017). Computational modeling probing the kinetics of the known plausible first generation oxidation steps (reactions R1–R5 in Figure 1) revealed that the mechanisms for these two monoterpenes diverge at the nitrooxy–alkoxyl radical (RO) intermediate (reaction R5). The α-pinene-derived RO reacts with cleavage of the C−C bond α to the nitrate group, followed by rapid decomposition into the closed-shell pinonaldehyde plus NO_2, whereas in the Δ-carene-derived RO cleavage preferentially occurs at the C−C bond β to the nitrate group, generating a primary alkyl radical (Kurtén et al., 2017). Thus, bond scission in the former terminates the organic radical chain, while in the latter it produces a ring-opened alkyl radical that, upon O_2-addition, can undergo further uni- and bimolecular reactions, eventually leading to low enough volatility products to contribute to SOA (Draper et al., 2019).

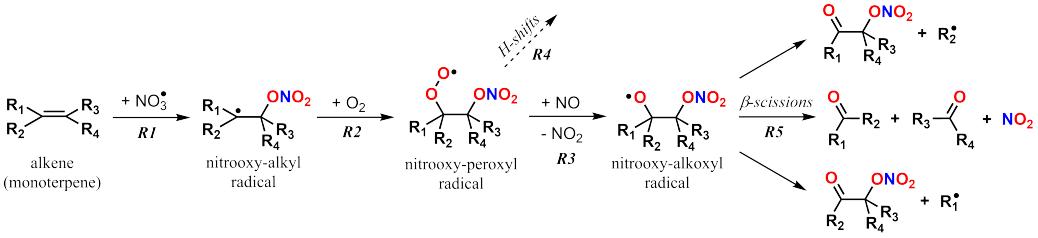

Figure 1: Monoterpene + NO_3 reactions

In this study, we expand upon the work by Kurtén et al. (2017) to five more cyclic monoterpenes: limonene, α-thujene, sabinene, β-pinene, and camphene, to better characterize the structural nuances that lead to important mechanistic differences. For the bicyclic terpenes (α-thujene, sabinene, β-pinene, and camphene), a ring-opening reaction from rearrangement of the original nitrooxy–alkyl radical (which can also be defined as β-scissions) may be possible in addition to the alkoxyl radical β-scissions that were the focus of Kurtén et al. (2017), and therefore we focus on both of these types of reactions here. Understanding the branching at these two steps provides indicators for the types of reactions that remain available for each monoterpene, or conversely, the monoterpenes that are likely to terminate to a closed-shell product earlier than others, producing higher volatility products and in general, lower SOA yields. We note, however, that these closed-shell products can themselves undergo NO_3 radical attack, potentially contributing to SOA yields via second generation oxidation.

Large scale modeling approaches for predicting aerosol budgets must simplify this complex chemistry by necessity and typically do so by lumping all monoterpenes and parameterizing the "monoterpene SOA yield" using laboratory yields from a single representative model system (often α-pinene). This approach is problematic, however, given the enormous variability of SOA yields for different monoterpene and oxidation combinations (Thomsen et al., 2021). One modeling study showed that by adjusting just the model monoterpene system, using β-pinene + NO_3 to represent all monoterpene + NO_3 yields instead of α-pinene, more than 50% of the estimated monoterpene-derived SOA in the US was found to originate from NO_3 oxidation (Pye et al., 2015). Combined with Kurtén et al. (2017), the present study elucidates the ring-opened fate of six of the eight most abundantly emitted monoterpenes globally as well as α-thujene as a structural analog to α-pinene. This dataset is a significant milestone in understanding the gas-phase mechanisms that do or do not lead to SOA and may be a jumping off point to reframe the simpler monoterpene SOA yield parameterizations necessary to improve larger scale modeling efforts.

2. Methods

In order to assess the fate of the alkyl and alkoxyl radical intermediates, we have calculated the reaction energy barrier for each possible β-scission using quantum chemical methods, then derived the corresponding rate coefficients using Transition State Theory (TST). From these rate coefficients, we are able to calculate branching ratios for these reaction channels. For each monoterpene studied, we assumed only the dominant NO_3 addition pathway (Wängberg et al., 1997; Yeh et al., 2015; Wayne et al., 1991) leading to the more stable tertiary alkyl radical. We explored the RO β-scission reactions for each nitrooxy–alkoxyl stereoisomer (four for endocyclic nitrate RO and two for exocyclic nitrate RO). Reactions leading to elimination of a methyl radical are expected to be negligible and were therefore not included. Concerning nitrooxy–alkyl radical ring-opening reactions, we explored only those involving the opening of the smaller ring in bicyclic monoterpene-derived species, including every $RONO_2$ stereoisomer (two for endocyclic nitrate adducts and one for exocyclic nitrate adducts). Nitrooxy–alkoxyl reactant stereoisomer structures are shown in Figure 2, and the nitrooxy–alkyl stereoisomers correspond to the same structures, but omitting the alkoxyl stereocenter.

Rate coefficients were calculated using the procedure described in Møller

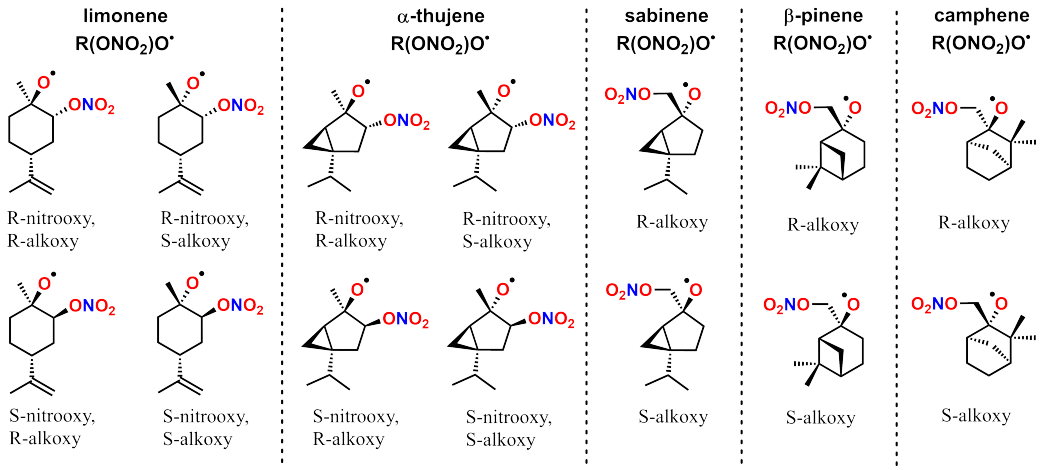

Figure 2: Molecular structure of nitrooxy–alkoxyl stereoisomers derived from the monoterpenes assessed in this study. Parent monoterpene enantiomers are (+)-limonene, (+)-α-thujene, (-)-sabinene, (-)-β-pinene, and (-)-camphene.

et al. (2016) for peroxyl radical H-shift reactions, and later benchmarked for alkoxyl radical β-scission reactions (Zhao et al., 2022). Briefly, systematic conformer sampling of each reactant, product, and transition state species was performed with Spartan v. 16 software (Spartan'16, 2016) using the Merck Molecular Force Field (MMFF94) method (Halgren, 1999). The keywords KEEPALL and FFHINT were applied to the conformer search to ensure all conformers were stored in the output and that a neutral charge was applied to the radical center of each molecule. Geometry optimizations and frequency calculations were then performed with Gaussian 09 software (Frisch et al., 2009) using density functional theory (DFT). Prior to conformer sampling, an arbitrary transition state structure for each reaction of interest was optimized at the B3LYP/6-31+G(d) (Becke, 1993; Lee et al., 1988; Ditchfield et al., 1971; Hehre et al., 1972; Hariharan & Pople, 1973; Clark et al., 1983) level, constraining the length of the bond being broken. The unconstrained transition state geometry was then found via a transition state optimization, also at the B3LYP/6-31+G(d) level, and this geometry was the input for the transition state conformer sampling with the breaking bond length again constrained. Each identified conformer was then optimized at the B3LYP/6-31+G(d) level (constrained optimization followed by

saddle-point search for transition states). Unique conformers (determined based on electronic energy and dipole moment (Møller et al., 2016)) within 2 kcal/mol of the lowest energy conformer were then re-optimized at the ωB97XD/aug-cc-pVTZ level (Chai & Head-Gordon, 2008; Dunning Jr, 1989; Kendall et al., 1992). Finally, restricted open-shell coupled cluster ROHF-DLPNO-CCSD(T)-F12/cc-pVTZ-F12 (Kumar et al., 2020; Hansen et al., 2011; Saitow et al., 2017; Peterson et al., 2008) single-point energy calculations were performed on the lowest energy conformer of each species using Orca 4.2.1 (Neese, 2012, 2018) to obtain more accurate energy treatment. For the lowest energy conformer of each transition state, intrinsic reaction coordinate (IRC) calculations were run at the B3LYP/6-31+G(d) level to determine the reactant and product conformer connected to the transition state. These obtained geometries were then optimized at the ωB97XD/aug-cc-pVTZ level and forward/reverse energy barriers were used in conjunction with the imaginary frequency of the transition state to calculate the Eckart tunneling correction factor (Eckart, 1930). Rate coefficients were then calculated using lowest-conformer TST (Eyring, 1935). The multi-conformer approach to transition state theory (MC-TST), as described in (Møller et al., 2016; Zhao et al., 2022), was also used to obtain rate coefficients of alkoxyl scissions for limonene- and sabinene-derived species. Due to increased computational costs, we chose to employ the full MC-TST treatment only to one exocyclic $RONO_2$ system (sabinene) and one endocyclic $RONO_2$ system (limonene). In the cases where we attempted to understand reactivity trends in terms of stereoelectronic and/or steric effects, we performed Natural Bonding Orbital (NBO) (Carpenter & Weinhold, 1988) analyses with the NBO 7.0 package (NBO 7.0, 2018) interfaced with Gaussian.

For the bicyclic monoterpenes where the initial alkyl radical may rearrange to open the minor 3-, 4-, or 5-membered ring (i.e. α-thujene, sabinene, β-pinene, and camphene) reaction dynamics were simulated using the Master Equation Solver for Multi Energy-well Reactions (MESMER) software (Glowacki et al., 2012) to determine whether the ring-opening channel is likely to be competitive with peroxyl radical formation via O_2-addition. The zero-point corrected energies were calculated at the ROHF-DLPNO-CCSD(T)-F12/cc-pVTZ-F12//ωB97XD/aug-cc-pVTZ level, and vibrational frequencies, and rotational constants were calculated at the ωB97XD/aug-cc-pVTZ level. Simulation conditions and parameters used were similar to those employed in simulation for the α-pinene ring-break analog Kurtén et al. (2017). Inverse Laplace Transform (ILT) method was used to model

the NO_3-addition reaction, assuming a barrierless association, since no TS was available for those. O_2-addition reactions were assigned to the initial nitrooxy–alkyl radical and to its ring-opening product, and were treated as simple bimolecular sinks. Bimolecular rate coefficients used were $1*10^{-10}$ and $6*10^{-12}$ cm^{-3} $molecule^{-1}$ s^{-1} for NO_3 addition and O_2 addition respectively. The ring-break reaction, for which a TS was calculated, was modeled using standard Rice-Ramsperger-Kassel-Marcus (RRKM) theory with Eckart tunneling correction. The exponential-down model was used to treat collisional energy transfer, with parameter $\Delta E_{\text{down}} = 225$ cm^{-1}. The Lennard–Jones parameter values used (Table S5 in the SI) were estimated using the procedure described in (Gao et al., 2016; Tee et al., 1966), based on a group-additivity method for deriving pure-compound critical properties by Joback and Reid (1987) (Joback & Reid, 1987). N_2 was assigned as the bath gas, with Lennard–Jones parameters $\epsilon = 91.85$ K and $\sigma = 3.919$ Å. Simulated energy grains spanned 50 kBT above the highest stationary point, with grain size value of 50 cm^{-1}. Very high NO_3 concentration (10^{15} molecules cm^{-3}) was used to ensure rapid formation of the modeled monoterpene-ONO_2 intermediate ($RONO_2$). This unrealistic value was used solely for ease of simulation and has no effect on the other reaction steps. O_2 concentration used was $5.16 * 10^{18}$ molecules cm^{-3} (0.21 atm). The sensitivity of product yields to uncertainty in model parameters was analysed with a procedure similar to the one described in (Zádor et al., 2023). For each monoterpene, the master equation calculation was re-run 500 times, applying to each new run a random variation in parameter values within pre-selected uncertainty ranges. Zero-point corrected energy variation was within ± 0.25 and ± 0.5 kcal mol^{-1} for wells and transition states respectively. For variations in vibrational frequencies (including imaginary ones), Lennard–Jones parameters, ΔE_{down} parameters, and bimolecular rate coefficients, we apply a random multiplicative factor ($\overset{\times}{\div}$a) within a log-normally distributed uncertainty range ($[1/a, a]$). We chose a multiplicative factor of $\overset{\times}{\div}3$ for the bimolecular rate coefficients, and a multiplicative value of $\overset{\times}{\div}1.2$ for the other parameters. In the case of (real) vibrational frequencies, a single random factor is used for all modes of a species, which correspond to the factor applied to a hypothetical mode with a vibrational wavenumber value of 100 cm^{-1}. This factor is dampened or amplified when applied to modes with higher or lower frequencies respectively, using a dampening function (Equation S3 in the SI).

3. Results and Discussion

3.1. Nitrooxy Alkyl Radical Ring Opening Reactions

We start by comparing the branching ratios for the ring-opening rearrangement of our initial nitrooxy–alkyl radical versus O_2-addition. O_2 addition to alkyl radicals is extremely fast in the atmosphere (pseudo-1st order rate $\sim 10^7$ s^{-1}) (Park et al., 2004) due to the high abundance of O_2 and therefore this is generally assumed to be the dominant path during VOC oxidation. However, radical addition to an unsaturated VOC is an exothermic process, and the some of that extra energy may propel the adduct to overcome the energy barrier of a subsequent unimolecular reaction before thermalization (i.e. dissipation of the extra energy into the bath gas via collisional energy transfer). For bicyclic compounds where the initial radical center is α to a strained ring, it may be energetically favorable to cleave an adjacent C−C bond to release that ring strain, resulting in a rearrangement of the radical and formation of a new double bond to maintain saturation. Figure 3 shows these reactions for each of the bicyclic monoterpenes studied here. Details on the energetics of each of these reactions, as well as TST rate coefficients and RRKM-ME product yields at 298 K and 1 atm are shown in Table 1.

Table 1: Zero-point corrected energies for the $RONO_2$ ring-opening transition states (TS) and their corresponding parent monoterpene + NO_3, relative to the nitrooxy–alkyl adducts, calculated at the RO-DLPNO-CCSD(T)-F12/cc-pVTZ-F12//ωB97XD/aug-cc-pVTZ level, and yield of ring-opening products calculated with RRKM-ME, at 298.15 K and 1 atm. Thermal rate coefficients calculated using Lowest-Conformer Transition State Theory (LC-TST) at 298.15 K, and product yields assuming a rate coefficient of 10^{-12} cm^3 $molecule^{-1}$ s^{-1} for the competing $RONO_2 + O_2$ reaction. Standard deviations ($+\sigma/-\sigma$) calculated from the logit-transformed distribution of branching ratios.

Monoterpene (MT)	$E_{v=0}$ (kcal mol^{-1})		Yield (%) ($+\sigma/-\sigma$)		k_{TST} (s^{-1})
	MT + NO_3	TS	RRKM-ME	TST	
sabinene	23.23	9.64	86 (+13/−64)	12	6.94×10^5
α-thujene (R)	23.92	12.84	11 (+34/−9)	∼0	3.09×10^3
α-thujene (S)	25.29	12.50	31 (+53/−26)	∼0	9.91×10^3
β-pinene	22.88	13.01	10 (+24/−8)	∼0	1.68×10^3
camphene (R1)	21.79	30.12	∼0	∼0	3.70×10^{-10}
camphene (R2)	21.79	24.89	∼0	∼0	2.84×10^{-6}
camphene (R3)	21.79	42.32	∼0	∼0	5.55×10^{-19}

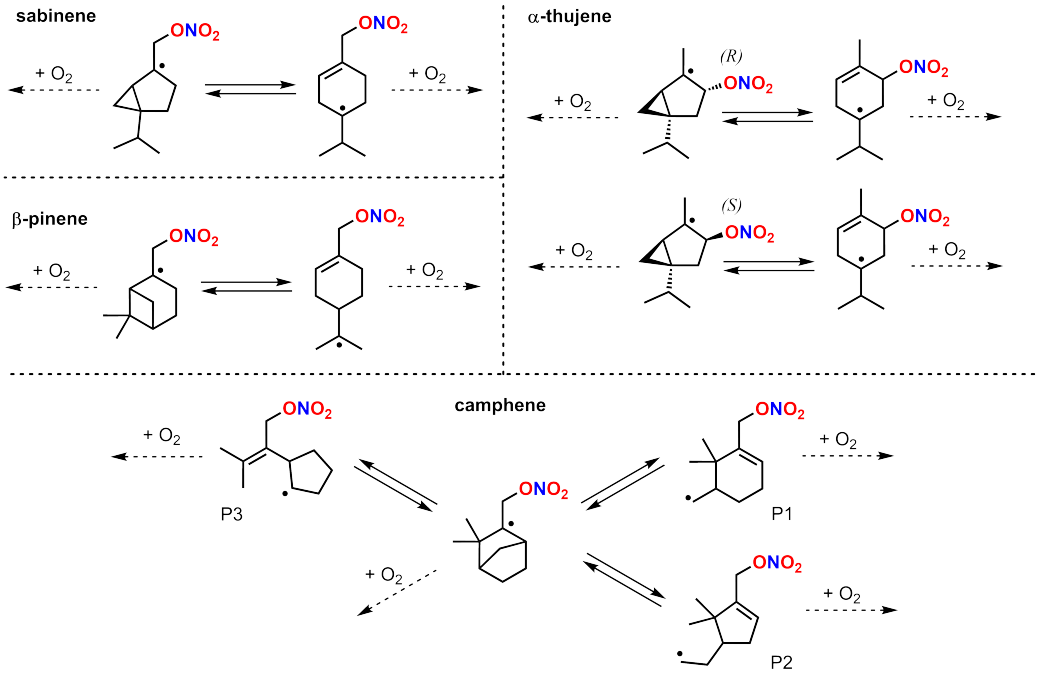

Figure 3: Ring opening radical rearrangement reactions for nitrooxy–alkyl radicals from bicyclic monoterpenes.

The time evolution of species distribution obtained with RRKM-ME calculations for the $RONO_2$ derived from sabinene, β-pinene and α-thujene are shown in Figure 4. Results from the camphene-derived species are omitted since virtually no ring-opening product is observed. We can see that the relative contribution from this ring-opening reaction is partly controlled by the amount of ring strain released. Due to the lesser strain relief, opening of a 5-membered ring cannot compete with O_2 addition, as is the case with camphene. However, this ring-opening pathway becomes significant for β-pinene, with a yield of 10%, and even predominant for sabinene, with a yield of 86%. For α-thujene, this pathway appears to be less important than observed for sabinene, despite also involving opening of a highly strained 3-membered ring, showing a yield of 11% and 31% for the (R)- and (S)-$RONO_2$ isomers respectively.

Stereoelectronic effects offer a possible explanation for this difference. In all three $RONO_2$ species (from sabinene and α-thujene) the radical center is

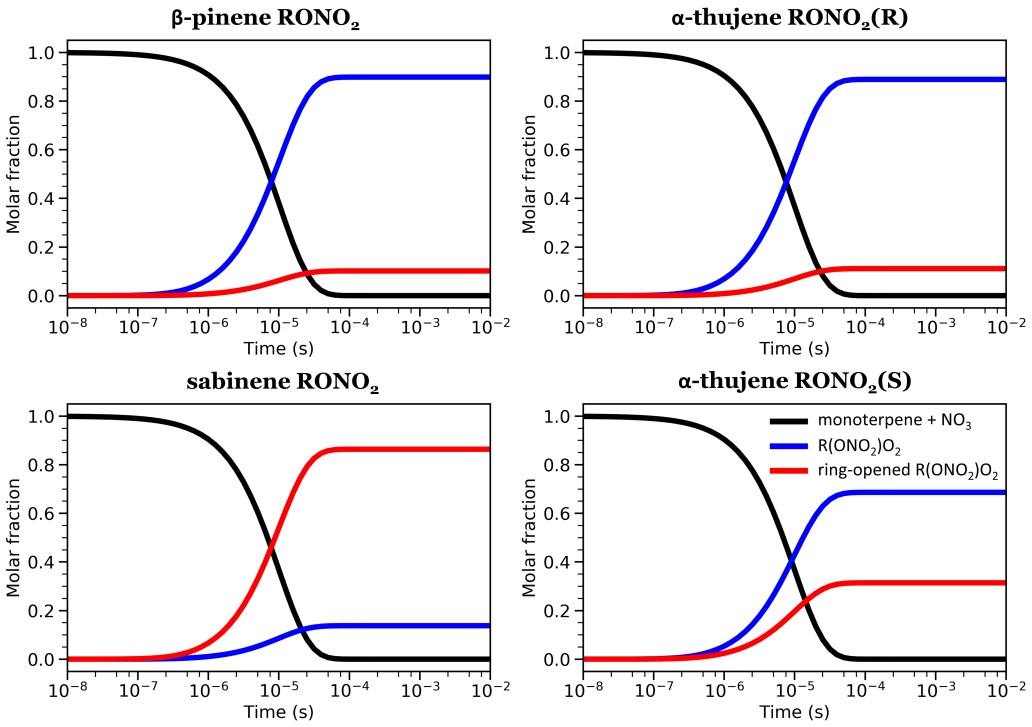

Figure 4: RRKM-ME simulated time series of species distributions for bicyclic nitrooxy–alkyl radicals ($RONO_2$) reacting via ring-opening versus O_2-addition. Species whose molar fraction is displayed in blue and red correspond to products of O_2-addition to the intact alkyl radical ($R(ONO_2)O_2$) and to the ring-opened alkyl radical (ring-opened $R(ONO_2)O_2$) respectively.

β to the nitrate group, which in principle allows for hyperconjugative interaction between the singly-occupied p_C orbital and the empty σ^*_{CO} orbital. Electron delocalization brought by this interaction stabilizes the radical, but it requires the C−O bond to be at, or close to, a perpendicular orientation relative to the nodal plane of the p_C orbital, as shown in Figure 5a. In the sabinene $RONO_2$, the α-ONO_2 carbon is exocyclic, so rotation about its C−C bond is enough to produce a conformation which is optimal for hyperconjugation, even as the molecule is distorted towards the TS for ring-opening. On the other hand, the α-ONO_2 carbon in α-thujene is endocyclic, which constrains the orientation of the nitrate group, diminishing the effect of this stabilizing interaction. In the TS of the less reactive R-isomer, for exam-

ple, hyperconjugation nearly vanishes as the C−O bond assumes an almost parallel orientation relative to the radical center. These factors discussed above are reflected in the energy of the $p_C \rightarrow \sigma^*_{CO}$ interaction, calculated with second-order perturbation theory analysis of the Fock matrix in the NBO basis (Reed et al., 1988), shown in Table S1 in the SI. The same trend is observed for the electronic energies after removal of the off-diagonal Fock matrix element corresponding to said interaction. Comparison between the product yields obtained from RRKM-ME calculations and those estimated from TST rate coefficients reveals the importance of non-thermal kinetics for these reactions. The TST treatment, which does not account for the excess energy released during the preceding NO_3-addition, predicts ring-opening to be competitive only for the sabinene $RONO_2$ adduct, and with a yield about seven times lower (12%) than obtained with RRKM-ME. Considering an uncertainty factor of ∼5 in TST rate coefficients (associated with a ∼1 kcal mol^{-1} uncertainty in energy barrier heights), we estimate a maximum yield of ∼24% for the ring-opening rearrangement in sabinene's $RONO_2$ derivative, which is still lower than the yield calculated with RRKM-ME. For the second fastest ring-opening reaction (α-thujene's (S)-$RONO_2$ derivative), we estimate a maximum yield of only ∼0.4%, considering the uncertainty in the TST rate coefficient.

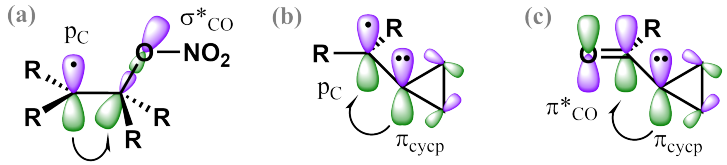

Figure 5: Stabilizing (hyper)conjugative interactions in studied nitrooxy–alkyl ($RONO_2$) radicals and nitrooxy–alkoxyl ($R(ONO_2)O$) radicals. a) $p_C \rightarrow \sigma^*_{CO}$ interaction; b) $\pi_{cycp} \rightarrow p_C$; c) $\pi_{cycp} \rightarrow \pi^*_{CO}$ interaction.

3.2. Nitrooxy Alkoxyl Radical β-scission Reactions

The reaction labeling scheme for nitrooxy–alkoxyl β-scission reactions is presented in Figure 6. Rate coefficients were calculated for the "right" (Rβ1) and "left" (Rβ2) C−C bond scissions for endocyclic monoterpenes and for the "right," "left," and "top" (Rβ3) C−C bond scissions for exocyclic monoterpenes with all molecules drawn in comparable orientation, as shown in Figure 2 above.

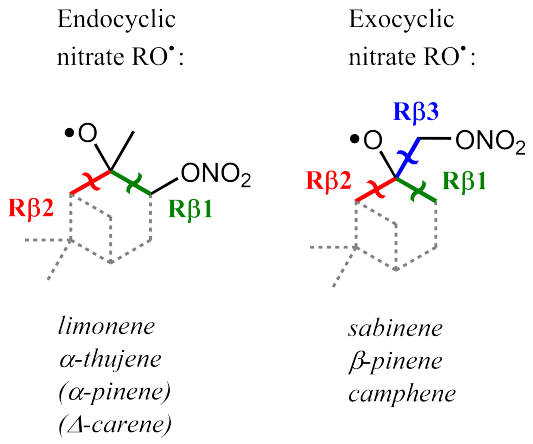

Figure 6: Reaction labeling scheme for nitrooxy–alkoxyl scission reactions.

In Table 2 we have compiled the zero-point corrected forward barriers, TST rate coefficients and branching ratios for each alkoxyl β-scission reaction studied. For completeness, we have also included the barriers and rate coefficients for α-pinene and Δ-carene taken from Kurtén et al. (2017). Rate coefficients estimated with MC-TST for β-scissions in the derivatives of limonene and sabinene are shown in Table S4 of the SI. In most cases, multi-conformer effects act to lower rate coefficient values by a similar magnitude. Consequently, their impact on product yields is predicted to be relatively small, changing at most by ∼3% when comparing results obtained with MC-TST and standard lowest-conformer TST. An uncertainty factor of ∼5 in rate coefficients estimated with TST translates into different product yield uncertainties for alkoxyl radicals derived from different monoterpenes. For example, the uncertainty in product yields is relatively small for sabinene (Δyield = ∼17%) and camphene (Δyield = ∼6%), and negligible for α-thujene (Δyield = ∼0%), whereas it is larger for limonene (Δyield = ∼38%) and β-pinene (Δyield = ∼46%).

Energy barriers, rate coefficients and branching ratios predicted using a structure–activity relationship (SAR) developed for this class of reactions (Vereecken & Peeters, 2009) are shown in Table 3 for comparison. For α-thujene and limonene, the SAR accurately predicts the relative favorability of each β-scission pathway, where the release of (5- or 6-membered) ring strain and extra stability afforded to the transition state by α-ONO_2 substitution to the developing radical center (as well as the destabilization brought

Table 2: Forward barrier heights (difference between transition state and reactant zero-point corrected energies at the RO-DLPNO-CCSD(T)-F12/cc-pVTZ-F12//ωB97XD/aug-cc-pVTZ level), rate coefficients calculated using Lowest-Conformer Transition State Theory (LC-TST) at 298.15 K, and product yields for the nitrooxy–alkoxyl beta-scission reactions at 298.15 K of 7 cyclic monoterpenes. Limonene, α-thujene, sabinene, β-pinene, and camphene were calculated in this study. [a]: Values for α-pinene and Δ-carene are reproduced from (Kurtén et al., 2017) for completeness.

Monoterpene (stereoisomer)	$\Delta^{\ddagger}E_0$ (kcal mol^{-1})			k_{TST} (s^{-1})			Yield (%)		
	Rβ1	Rβ2	Rβ3	Rβ1	Rβ2	Rβ3	Rβ1	Rβ2	Rβ3
limonene (R,R)	9.85	12.04	-	9.85×10^5	3.91×10^3	-	100	0	-
limonene (R,S)	10.00	11.79	-	7.58×10^5	9.43×10^4	-	89	11	-
limonene (S,R)	9.46	11.91	-	1.61×10^6	2.58×10^4	-	98	2	-
limonene (S,S)	9.10	10.79	-	1.49×10^6	1.36×10^5	-	92	8	-
α-thujene (R,R)	7.20	16.21	-	8.10×10^7	20.4	-	100	0	-
α-thujene (R,S)	7.90	16.19	-	1.69×10^7	6.36	-	100	0	-
α-thujene (S,R)	7.60	15.28	-	3.49×10^7	78.3	-	100	0	-
α-thujene (S,S)	7.96	15.42	-	1.85×10^7	45.3	-	100	0	-
sabinene (R)	10.42	15.98	12.58	1.99×10^5	20.3	8.09×10^3	96	0	4
sabinene (S)	9.73	15.82	11.70	7.74×10^5	25.3	2.34×10^4	97	0	3
β-pinene (R)	10.84	11.25	9.63	1.14×10^5	3.83×10^4	9.92×10^5	10	3	87
β-pinene (S)	10.54	12.92	12.33	5.80×10^4	3.66×10^3	6.93×10^3	85	5	10
camphene (R)	1.59	4.27	11.41	2.44×10^{11}	3.13×10^9	3.49×10^4	99	1	0
camphene (S)	2.85	5.81	14.79	2.94×10^{10}	3.42×10^8	1.37×10^2	99	1	0
α-pinene (R,R)[a]	6.1	10.6	-	1.7×10^8	1.3×10^5	-	100	0	-
α-pinene (R,S)[a]	4.8	9.4	-	1.5×10^9	3.6×10^6	-	100	0	-
α-pinene (S,R)[a]	6.7	10.4	-	7.5×10^7	3.7×10^5	-	100	0	-
α-pinene (S,S)[a]	8.6	10.5	-	2.2×10^6	1.0×10^5	-	96	4	-
Δ^3-carene (R,R)[a]	8.4	7.4	-	8.2×10^6	2.7×10^7	-	23	77	-
Δ^3-carene (R,S)[a]	9.2	8.3	-	1.7×10^6	8.4×10^6	-	17	83	-
Δ^3-carene (S,R)[a]	8.4	8.4	-	3.3×10^6	6.2×10^6	-	35	65	-
Δ^3-carene (S,S)[a]	8.6	8.1	-	2.6×10^6	9.0×10^6	-	22	78	-

by a developing radical center on a cyclopropyl group in α-thujene) leads to

the right side scission (Rβ1, see Figure 6) being most favorable, leading to loss of NO_2 and oxidative chain termination. However, the SAR predictions are less accurate for the other monoterpenes studied here. The SAR correctly predicts the most favorable scission pathway for sabinene but suggests opposite relative favorability for the other two channels. For β-pinene and camphene, the SAR does not predict the lowest energy pathway calculated here. These observed inconsistencies indicate that the bicyclic structure of these monoterpenes may introduce additional layers of complexity not fully incorporated into the SAR.

Table 3: Predicted forward barrier heights based on a SAR for the nitrooxy–alkoxyl β-scission reactions at 298.15 K of studied cyclic monoterpenes.

Parent Monoterpene	E_b (kcal mol^{-1})			k_{SAR} (s^{-1})			Yield (%)		
	Rβ1	Rβ2	Rβ3	Rβ1	Rβ2	Rβ3	Rβ1	Rβ2	Rβ3
limonene	6.5	9.3	15.9	2.92×10^8	2.72×10^6	3.93×10^1	99	1	0
α-thujene	4.6	9.3	15.9	7.96×10^9	2.72×10^6	3.93×10^1	100	0	0
sabinene	6.9	9.3	13.1	1.58×10^8	2.72×10^6	4.45×10^3	98	2	0
β-pinene	9.3	5.3	13.1	2.72×10^6	2.19×10^9	4.45×10^3	0	100	0
camphene	2.3	2.2	13.1	4.00×10^{11}	4.63×10^{11}	4.45×10^3	46	54	0
α-pinene	6.5	5.3	15.9	2.92×10^8	2.19×10^9	3.93×10^1	12	88	0
Δ-carene	6.5	9.3	15.9	2.92×10^8	2.72×10^6	3.93×10^1	99	1	0

In general, we find that β-scissions resulting in a radical center on a 3-, 4-, or 5-membered ring structure have the highest energy barrier, whereas the SAR indicates β-cycloalkyl substitution (except for cyclopropyl) significantly decreases the overall β-scission barrier, tipping the scales over other substituent effects (Vereecken & Peeters, 2009). Interestingly, for β-pinene we find all three β-scission pathways are competitive and each stereoisomer has a preference for a different pathway — the S-alkoxyl isomer preferentially cleaving the right side C−C bond (Rβ1) opening up the 6-membered ring and the R-alkoxyl isomer preferentially cleaving the top C−C bond (Rβ3), eliminating nitrooxymethyl radical ($H_2C{-}ONO_2$) and keeping the 6-membered ring intact. Of all of the exocyclic nitrate compounds, we observe Rβ3 to be more favorable than the β-scission that would result in a radical centered on a strained ring (Rβ2), though the SAR predicts it to be the most favorable

in β-pinene. Perhaps these observations indicate that the SAR may underestimate the destabilizing effect of β-cycloalkyl substitution and/or stabilizing effect of β-ONO_2 substitution. For reactions Rβ2 in sabinene, α-thujene and β-pinene, a possible source for the underestimation of the energy barrier by the SAR is the fact that, in these monoterpenes, the 3- or 4-membered ring contains a quaternary carbon, whose bulky substituents may prevent the ring from adapting its geometry to properly accommodate the radical center.

Additionally, experimental evidence in the bulk liquid phase indicates that an α-cyclopropyl substituent enhances the lability of other $C_\alpha - C_\beta$ bonds (i.e. α-cyclopropyl acts as an assisting substituent) in alkoxyl β-scission reactions (Bietti et al., 2005). The C−C bonding orbitals in cyclopropane have significant p character, and may interact with p or π orbitals in adjacent groups via conjugation. The stabilization brought by this interaction is maximized if the cyclopropyl group assumes a bissected conformation with respect to the nodal plane of the acceptor p or π orbital (see Figure 5 (b)), allowing for optimal overlap. Thus, the transition state of a β-scission may receive a stability boost from overlap of the forming π^*_{CO} orbital with one of the Walsh-type π_{cycp} orbitals in an α-cyclopropyl substituent (Figure 5c) (Bietti et al., 2005; Roth & Herbertz, 1993). This effect, whose contribution is absent in the SAR, could in principle assist the right (Rβ1) and/or top (Rβ3) side scissions for α-thujene and sabinene. However, further inspection of the transition states of reactions Rβ1 for sabinene and α-thujene reveals that, perhaps due to constraints imposed by the larger ring, their structures deviate strongly from a bissected conformation (Table S3 in the SI), suggesting that the $\pi_{cycp} \rightarrow \pi^*_{CO}$ interaction is minor in these systems. The bulk phase experiments by (Bietti et al., 2005) suggest that an effect similar to the one described for α-cyclopropyl substitution is not observed for α-cyclobutyl substituents however, and those β-scissions are governed by radical stability alone.

3.2.1. Proposed Fate of Each Monoterpene

Proposed mechanisms for each monoterpene studied (as well as α-pinene and Δ-carene reproduced from Kurtén et al. (2017) for completeness) are shown in Figures 7-11. We can see that certain structural features favor specific reaction pathways. However, we also see that each unique permutation of similar structural features leads to each monoterpene having its own unique reactivity beginning early in the oxidative chain. It logically follows then that the SOA yield from each monoterpene would be different. Broadly,

we see that monoterpenes with the potential for multiple generations of radical propagation reactions are the same monoterpenes that exhibit moderate to high SOA yields in the laboratory (Fry et al., 2014; Ng et al., 2017). Conversely, α-pinene, which has been shown to have negligible SOA yields from NO_3-initiated oxidation, has a dominant termination pathway (RO scission leading to NO_2 loss) quite early in its oxidative chain, suggesting it will have a significantly lower yield of low volatility products that would be expected to dominate SOA formation and growth. Experimental SOA yields have not yet been measured for α-thujene or camphene with NO_3 radical, but mechanistically we would expect α-thujene to fall on the lower end of the spectrum due to the availability of the analogous NO_2 loss seen in α-pinene, and we would expect camphene to fall on the higher end of the spectrum since its dominant scission pathways continue organic radical propagation and are calculated to be extremely fast, even compared to the quite fast β-scission pathways of the other monoterpenes studied. Experimental work by (Dam et al., 2022) indeed suggests that, like with α-pinene, NO_3-initiated oxidation of α-thujene leads to minimal aerosol particle yields.

Limonene

Beginning with the simplest monoterpene studied here, insofar as it is monocyclic and therefore does not have the additional mechanistic complexity afforded by a secondary ring structure, the proposed fate of limonene is shown in Figure 7. We assume NO_3 addition will occur over the endocyclic double bond as shown by previous studies (Spittler et al., 2006), and, to the best of our knowledge, no available alkyl radical rearrangement pathway exists, so we consider just the right (Rβ1) and left (Rβ2) side alkoxyl scission reactions. Calculated rate coefficients indicate a vast majority (ca. 89–100%) of limonene intermediates will favor the Rβ1 scission, leading, via subsequent NO_2 loss, to the closed-shell endolim. While the non-dominant Rβ2 scission produces a primary alkyl radical that is expected to undergo further generations of organic radical propagation, the dominance of the pathway leading to an early organic radical termination might suggest a fairly low SOA yield and organonitrates yield. However, limonene has an additional double bond, which would allow initiation of a second generation NO_3 radical oxidation. Endolim(ONO_2)OOH and endolim(ONO_2)OH have both been observed in experiments (Faxon et al., 2018), and their precursor RO_2 and RO intermediates, being free from the constraints of a cyclic structure, are likely susceptible to additional organic radical propagation reactions leading

to even more highly oxidized organonitrates (Draper et al., 2019), supporting the relatively high SOA and organonitrates yield observed for limonene (Fry et al., 2014). Moreover, second generation oxidation could also be initiated via abstraction of the aldehydic hydrogen in endolim, with potential to produce highly-functionalized products. NO_3 radical attack on the aldehyde group, however, is probably less important than attack on the C−C double bond.

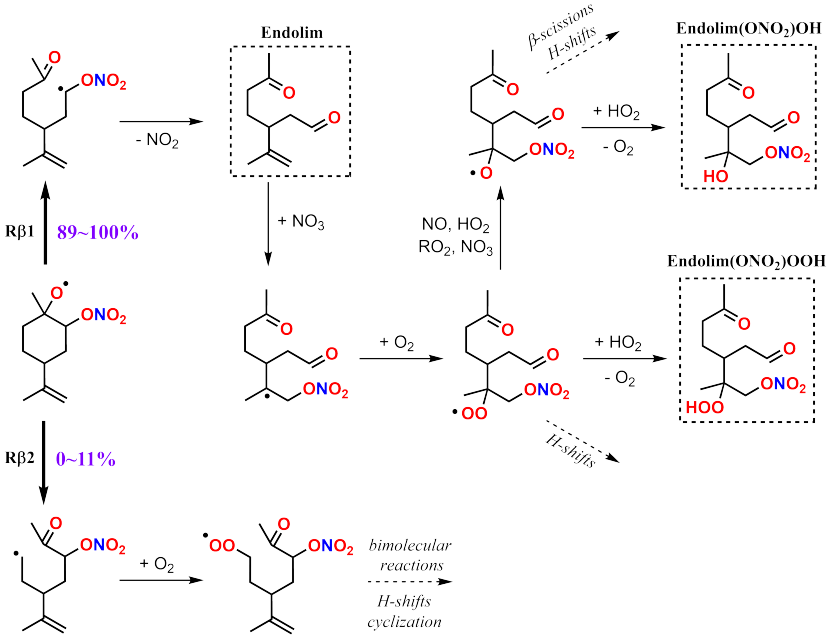

Figure 7: Proposed fate of limonene + NO_3 beginning from the first generation nitrooxy–alkoxyl radical. Bold arrows show the β-scission reactions studied here, including calculated branching ratios. Dashed boxes indicate selected products observed experimentally.

α-Thujene

Next we show our proposed mechanism for α-thujene in Figure 8. Based on the structural similarities to α-pinene (location of strained secondary ring with respect to double bond) we expected α-thujene to have a similar fate to that of α-pinene proposed in Kurtén et al. (2017) — dominance of the Rβ1 alkoxyl scission resulting in loss of NO_2 and early termination of the oxidative chain. However, since α-thujene has a 3-membered ring instead of a 4-membered ring, the additional ring strain is significant enough that the

earlier alkyl ring-opening radical rearrangement reaction is competitive, with a yield of 11–31%. This radical rearrangement allows for additional radical propagation reactions (e.g. via RO_2 cyclization) as well as initiation of a second oxidative chain via NO_3 radical addition to the newly formed double bond, which could lead to a much larger distribution of highly oxidized products than would be observed for α-pinene. For the 69–89% that do undergo the more typical O_2 addition and alkoxyl scission, the right side (Rβ1) scission is predicted to be the only competitive pathway. This pathway produces a non-trivial yield of the fairly volatile closed-shell product α-thujonaldehyde, which may lessen the overall SOA yield from α-thujene.

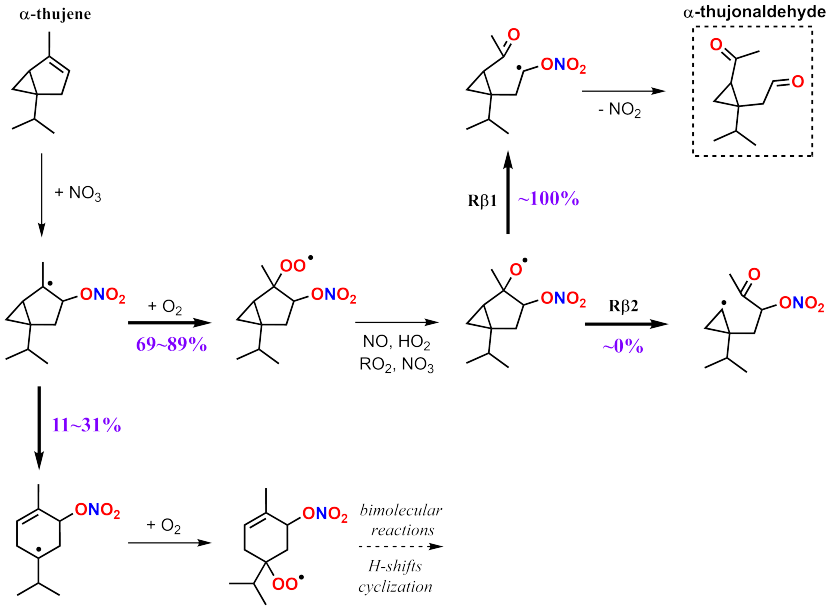

Figure 8: Proposed fate of α-thujene + NO_3 beginning from the first generation nitrooxy–alkyl radical. Bold arrows show the reactions studied here, including calculated branching ratios. Dashed boxes indicate predicted closed-shell products.

Sabinene

Sabinene (Figure 9) differs from α-thujene only in its exocyclic double bond compared to α-thujene's endocyclic double bond. Since the most favorable NO_3 addition pathway results in the same tertiary radical center as α-thujene, sabinene also undergoes the alkyl radical ring-opening reaction, but with a much higher yield (86%), leading to further radical propagation and the

possibility for second generation NO_3 oxidation. Along the alkoxyl radical pathway for the other 14%, sabinene favors the right side (Rβ1) scission, with a yield of 96–97%. However, unlike in α-thujene, this pathway does not terminate the oxidative chain right away and instead forms a primary alkyl radical that can undergo additional radical propagation steps (e.g. via RO_2 1,6-H-shift from a tertiary carbon) leading to highly functionalized low volatility products. The β-scission leading to elimination of a nitrooxymethyl radical (Rβ3) is minor (3–4%), producing sabinaketone. Overall, these results suggest a fairly large SOA yield from sabinene oxidation initiated by NO_3 radical.

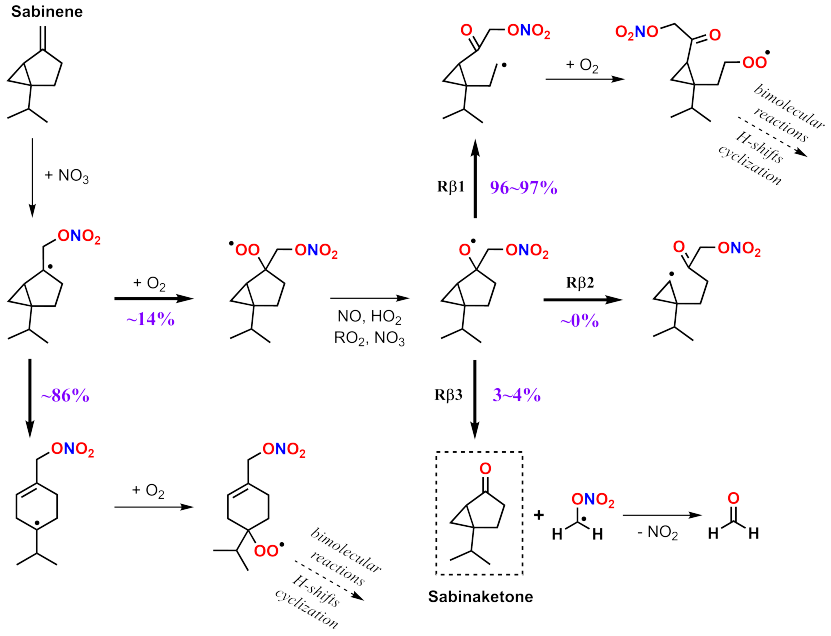

Figure 9: Proposed fate of sabinene + NO_3 beginning from the first generation nitrooxy–alkyl radical. Bold arrows show the reactions studied here, including calculated branching ratios. Dashed boxes indicate predicted closed-shell products.

β-Pinene

The mechanism for β-pinene oxidation is shown in Figure 10. RRKM-ME calculations indicate that the alkyl radical ring-opening reaction is minor but competitive, with 10% yield, contrasting with the results for α-pinene in Kurtén et al. (2017), whose analogous ring-opening reaction was predicted to

be negligible. Perhaps the stereoelectronic effects that explain the difference in reactivity between sabinene and α-thujene towards ring-opening, described in Section 3.1, may also apply here. The exocyclic nitrate group in the β-pinene RO allows for optimal $p_C \rightarrow \sigma^*_{CO}$ interaction, whereas the endocyclic nitrate in the α-pinene RO does not. Alkyl radical ring-opening is expected to lead to additional radical propagation steps (e.g. via RO_2 cyclization or 1,5-H-shift from an allylic carbon). Concerning further oxidation of the 90% that proceed without ring-opening, the alkoxyl radical channels are unique among the monoterpenes studied here insofar as all three β-scission pathways have significant branching ratios, and the most favorable pathway is different for the two RO stereoisomers — R-alkoxyl favoring Rβ3 (87%) and S-alkoxyl favoring Rβ1 (85%). This is due to a sharp difference in the energy barrier for reaction Rβ3 ($\sim$ 2.7 kcal mol^{-1}), for which steric effects, rather than stereoelectronic, may offer an explanation. As the RO molecule distorts towards the transition state in reaction Rβ3, the leaving nitrooxymethyl group experiences greater steric repulsion in the S-isomer than in the R-isomer, due to the group's proximity to the bulky dimethyl-substituted carbon in the former, which raises the reaction energy barrier. We find that the total steric exchange energy calculated with NBO Badenhoop & Weinhold (1997a,b) for these species (see Table S2 in the SI) agree with this hypothesis. In terms of subsequent chemistry, both the Rβ1 and Rβ2 pathways have potential for continued radical propagation, whereas the Rβ3 scission leads to the closed-shell nopinone. In one chamber study, however, nopinone was only measured in 1–2% yield (Hallquist et al., 1999). Due to steric congestion, we may expect that formation of the S-peroxyl (and thus S-alkoxyl) stereoisomer is favored over the R-peroxyl, which could explain the low yields of nopinone, but this is speculation and we are not certain what the actual distribution of RO_2 stereoisomers is likely to be.

Camphene

The mechanism for camphene oxidation is shown in Figure 11. Since its secondary ring structure is a 5-membered ring, camphene's initial oxidation seems to be driven less by the artifacts of a strained ring than the other bicyclic monoterpenes studied. Following the trend observed with secondary ring sizes, the smaller strain relief from opening of a 5-membered ring translates into higher energy barriers for alkyl radical rearrangement, so these channels cannot compete with O_2 addition. For alkoxyl radical β-scissions, our calculations indicate that the left side scission (Rβ2) leading to a rad-

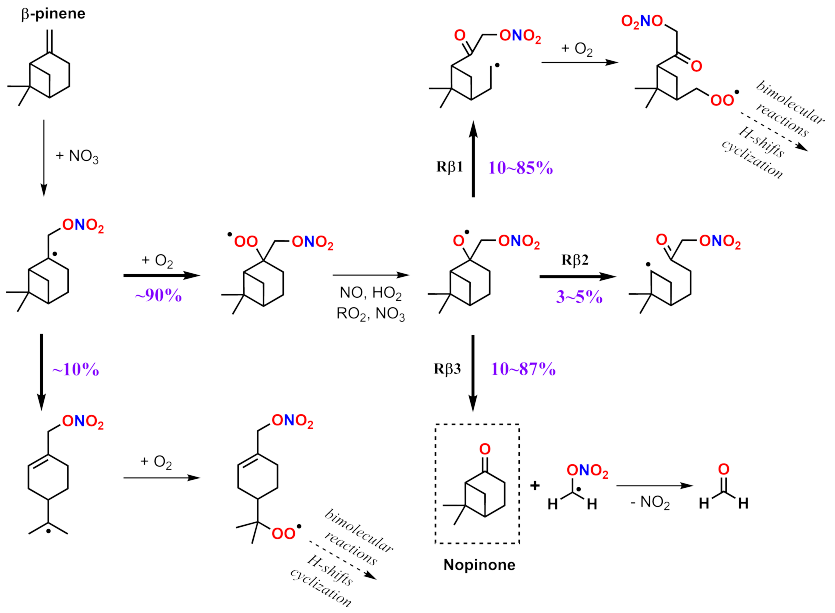

Figure 10: Proposed fate of β-pinene + NO_3 beginning from the first generation nitrooxy–alkyl radical. The first generation nitrooxy–alkoxyl radical is outlined in black. Bold arrows show the reactions studied here, including calculated branching ratios. Dashed boxes indicate predicted major product channels.

ical center on the cyclopentyl group is less favorable, with 1% yield, than the right side scission (Rβ1), which forms a tertiary alkyl radical with 99% yield. That said, in terms of absolute rate coeffcients, both of these pathways are faster than the dominant β-scission for any of the other monoterpenes studied here, due to a combination of ring strain relief and development of stabilized radical centers (tertiary or secondary alkyl radicals). Cleavage of the exocyclic C−C bond via Rβ3, leading to oxidative chain termination and formation of camphenilone, is a negligible channel. These results indicate a potential for high SOA yields from camphene oxidation initiated by NO_3 radicals, given that the major product (99%) may undergo further radical propagation reactions (e.g. via RO_2 1,5-H-shift from the intact cyclopentyl group).

α-Pinene and Δ-Carene

Analogous mechanisms for α-pinene and Δ-carene were published in Kurtén et al. (2017). Like α-thujene, α-pinene shows an overwhelmingly dominant

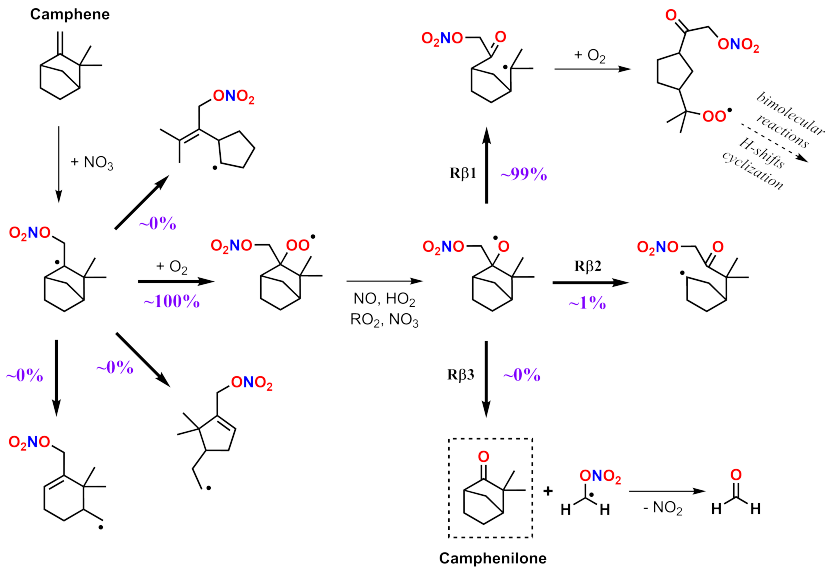

Figure 11: Proposed fate of camphene + NO_3 beginning from the first generation nitrooxy–alkyl radical. Bold arrows show the reactions studied here, including calculated branching ratios. Dashed boxes indicate predicted closed-shell products.

preference for right side β-scission that leads to NO_2 loss and early oxidative chain termination, consistent with its very low observed SOA yields, organonitrates yields (Fry et al., 2014), and high product yield of pinonaldehyde (Hallquist et al., 1999). Δ-Carene, continuing the trend of completely unique monoterpene reactivity, has a preference for the left side alkoxyl β-scission, perhaps due to reaction assistance by the cyclopropyl group as discussed in Section 3.2, but this time via a $\pi_{cycp} \rightarrow p^*_C$ interaction stabilizing the radical center. Incidentally, the produced α-cyclopropyl-substituted alkyl radical may be prone to fast ring-opening rearrangement, as seen for the sabinene and α-thujene nitrooxy alkyl radicals, thus providing two channels of further radical propagation reactions as well as an opportunity for second generation NO_3 oxidation. These later stage radical propagation reactions are explored in detail in Draper et al. (2019) and these pathways support the high SOA and organonitrates yields observed in chamber studies (Fry et al., 2014).

4. Conclusions

In this work we investigate the nitrooxy–alkyl ring-opening reactions and nitrooxy–alkoxyl β-scission reactions in the NO_3-initiated oxidation of five

monoterpenes (limonene, sabinene, α-thujene, β-pinene and camphene) with computational methods, and analyse their potential impact on the formation of atmospheric SOA particles. Our calculations indicate that the importance of alkyl radical rearrangements via opening of the secondary ring is partly dependent on the amount of ring strain released, their competition with O_2 addition increasing with decreasing ring sizes. This channel is dominant over O_2 addition for sabinene, minor yet competitive for α-thujene and β-pinene, and negligible for camphene. The difference in ring-opening yields observed for sabinene and α-thujene, both of which contain a 3-membered ring, suggest that due to stereoelectronic effects, the position of the nitrate group may also be controlling reactivity. A stabilizing hyperconjugative interaction involving the nitrate group is maintained during ring-opening for sabinene, whose nitrate group is exocyclic, whereas it diminishes for α-thujene, whose nitrate group is endocyclic. This effect may also explain the difference in reactivity between α-pinene and β-pinene, since ring-opening is a negligible channel in the former, according to study by Kurtén et al. (2017). Alkyl radical ring-opening may lead to enhanced SOA yields, given that the subsequently formed RO_2 radical is more susceptible to undergo radical propagation steps, and the newly formed C=C double bond allows for a second-generation NO_3 radical addition. As for the alkoxyl radical β-scission reactions, results from our calculations and those done by Kurtén et al. (2017) indicate that, in general, endocyclic nitrate species (e.g. derived from limonene, α-thujene and α-pinene) have a greater propensity to react via the channel leading to early termination of the oxidative chain (via NO_2 elimination), and thus relatively lower SOA yields. Ring-strain relief lowers the energy barrier for this reaction in endocyclic nitrate alkoxyl radicals, making it more favorable. Δ-Carene seems to be an exception in this case, reacting preferentially with formation of a primary alkyl radical, perhaps due to reaction assistance by α-cyclopropyl substitution to the new radical center. The experimental observation of high SOA yields from limonene oxidation by NO_3 radicals, which our calculations predict to lead to early termination, may be explained by second-generation NO_3-addition to the monoterpene's remaining C=C double bond. In contrast, no ring-strain relief offers assistance to the channel leading to NO_2 elimination in exocyclic nitrate species (e.g. derived from sabinene, β-pinene and camphene), which are instead expected to react forming open-chain alkyl radicals allowing for further radical propagation steps, and thus higher SOA yields. This study is a noteworthy achievement in unraveling the gas-phase processes that may contribute to the formation of SOA. Presented dataset

could serve as a starting point for deriving the more straightforward parameterizations of SOA yield from monoterpenes, crucial for enhancing the accuracy of larger-scale modeling endeavors.

Acknowledgement

This research was supported by funding from the US National Science Foundation (NSF; grant no. CHE-2004066). We acknowledge Research Council of Finland for funding (grant nos. 347775, 355966, and the center of excellence VILMA, grant no. 346369) and the CSC-IT Center for Science in Espoo, Finland, for computational resources.

Supporting Information

A supplement to this article will be available online, containing additional computational details, calculated energetics and cartesian coordinates for lowest-energy conformers. The raw data files produced during this research work will be uploaded to an online data repository (CERN Zenodo).

References

Atkinson, R. W., Mills, I. C., Walton, H. A., & Anderson, H. R. (2015). Fine particle components and health—a systematic review and meta-analysis of epidemiological time series studies of daily mortality and hospital admissions. *Journal of exposure science & environmental epidemiology*, *25*, 208–214.

Badenhoop, J., & Weinhold, F. (1997a). Natural bond orbital analysis of steric interactions. *The Journal of chemical physics*, *107*, 5406–5421.

Badenhoop, J., & Weinhold, F. (1997b). Natural steric analysis: Ab initio van der waals radii of atoms and ions. *The Journal of chemical physics*, *107*, 5422–5432.

Becke, A. D. (1993). A new mixing of hartree–fock and local density-functional theories. *The Journal of chemical physics*, *98*, 1372–1377.

Bianchi, F., Kurtén, T., Riva, M., Mohr, C., Rissanen, M. P., Roldin, P., Berndt, T., Crounse, J. D., Wennberg, P. O., Mentel, T. F. et al. (2019).

Highly oxygenated organic molecules (hom) from gas-phase autoxidation involving peroxy radicals: A key contributor to atmospheric aerosol. *Chemical reviews*, *119*, 3472–3509.

Bietti, M., Gente, G., & Salamone, M. (2005). Structural effects on the β-scission reaction of tertiary arylcarbinyloxyl radicals. the role of α-cyclopropyl and α-cyclobutyl groups. *The Journal of Organic Chemistry*, *70*, 6820–6826.

Carpenter, J., & Weinhold, F. (1988). Analysis of the geometry of the hydroxymethyl radical by the "different hybrids for different spins" natural bond orbital procedure. *Journal of Molecular Structure: THEOCHEM*, *169*, 41–62.

Chai, J.-D., & Head-Gordon, M. (2008). Long-range corrected hybrid density functionals with damped atom–atom dispersion corrections. *Physical Chemistry Chemical Physics*, *10*, 6615–6620.

Clark, T., Chandrasekhar, J., Spitznagel, G. W., & Schleyer, P. V. R. (1983). Efficient diffuse function-augmented basis sets for anion calculations. iii. the 3-21+ g basis set for first-row elements, li–f. *Journal of Computational Chemistry*, *4*, 294–301. doi:10.1002/jcc.540040303.

Dam, M., Draper, D. C., Marsavin, A., Fry, J. L., & Smith, J. N. (2022). Observations of gas-phase products from the nitrate-radical-initiated oxidation of four monoterpenes. *Atmospheric Chemistry and Physics*, *22*, 9017–9031.

Ditchfield, R., Hehre, W. J., & Pople, J. A. (1971). Self-consistent molecular-orbital methods. ix. an extended gaussian-type basis for molecular-orbital studies of organic molecules. *The Journal of Chemical Physics*, *54*, 724–728. doi:10.1063/1.1674902.

Draper, D. C., Myllys, N., Hyttinen, N., Møller, K. H., Kjaergaard, H. G., Fry, J. L., Smith, J. N., & Kurtén, T. (2019). Formation of highly oxidized molecules from no3 radical initiated oxidation of Δ-3-carene: A mechanistic study. *ACS Earth and Space Chemistry*, *3*, 1460–1470. doi:10.1021/acsearthspacechem.9b00143.

Dunning Jr, T. H. (1989). Gaussian basis sets for use in correlated molecular calculations. i. the atoms boron through neon and hydrogen. *The Journal of chemical physics*, *90*, 1007–1023. doi:10.1063/1.456153.

Eckart, C. (1930). The penetration of a potential barrier by electrons. *Physical Review*, *35*, 1303.

Eyring, H. (1935). The activated complex in chemical reactions. *The Journal of Chemical Physics*, *3*, 107–115.

Faxon, C., Hammes, J., Le Breton, M., Pathak, R. K., & Hallquist, M. (2018). Characterization of organic nitrate constituents of secondary organic aerosol (soa) from nitrate-radical-initiated oxidation of limonene using high-resolution chemical ionization mass spectrometry. *Atmospheric Chemistry and Physics*, *18*, 5467–5481.

Frisch, M., Trucks, G., Schlegel, H., Scuseria, G., Robb, M., Cheeseman, J., Scalmani, G., Barone, V., Mennucci, B., Petersson, G. et al. (2009). Gaussian 09, revision d. 01, gaussian, inc., wallingford ct. *See also: URL: http://www. gaussian. com*, .

Fry, J. L., Draper, D. C., Barsanti, K. C., Smith, J. N., Ortega, J., Winkler, P. M., Lawler, M. J., Brown, S. S., Edwards, P. M., Cohen, R. C. et al. (2014). Secondary organic aerosol formation and organic nitrate yield from no3 oxidation of biogenic hydrocarbons. *Environmental science & technology*, *48*, 11944–11953.

Gao, C. W., Allen, J. W., Green, W. H., & West, R. H. (2016). Reaction mechanism generator: Automatic construction of chemical kinetic mechanisms. *Computer Physics Communications*, *203*, 212–225.

Glowacki, D. R., Liang, C.-H., Morley, C., Pilling, M. J., & Robertson, S. H. (2012). Mesmer: an open-source master equation solver for multi-energy well reactions. *The Journal of Physical Chemistry A*, *116*, 9545–9560.

Griffin, R. J., Cocker III, D. R., Flagan, R. C., & Seinfeld, J. H. (1999). Organic aerosol formation from the oxidation of biogenic hydrocarbons. *Journal of Geophysical Research: Atmospheres*, *104*, 3555–3567.

Guenther, A., Jiang, X., Heald, C. L., Sakulyanontvittaya, T., Duhl, T. a., Emmons, L., & Wang, X. (2012). The model of emissions of gases and

aerosols from nature version 2.1 (megan2. 1): an extended and updated framework for modeling biogenic emissions. *Geoscientific Model Development*, *5*, 1471–1492.

Halgren, T. A. (1999). Mmff vii. characterization of mmff94, mmff94s, and other widely available force fields for conformational energies and for intermolecular-interaction energies and geometries. *Journal of Computational Chemistry*, *20*, 730–748.

Hallquist, M., Wängberg, I., Ljungström, E., Barnes, I., & Becker, K.-H. (1999). Aerosol and product yields from no3 radical-initiated oxidation of selected monoterpenes. *Environmental science & technology*, *33*, 553–559.

Hallquist, M., Wenger, J. C., Baltensperger, U., Rudich, Y., Simpson, D., Claeys, M., Dommen, J., Donahue, N., George, C., Goldstein, A. et al. (2009). The formation, properties and impact of secondary organic aerosol: current and emerging issues. *Atmospheric chemistry and physics*, *9*, 5155–5236.

Hansen, A., Liakos, D. G., & Neese, F. (2011). Efficient and accurate local single reference correlation methods for high-spin open-shell molecules using pair natural orbitals. *The Journal of chemical physics*, *135*, 214102.

Hariharan, P. C., & Pople, J. A. (1973). The influence of polarization functions on molecular orbital hydrogenation energies. *Theoretica chimica acta*, *28*, 213–222. doi:10.1007/bf00533485.

Hehre, W. J., Ditchfield, R., & Pople, J. A. (1972). Self—consistent molecular orbital methods. xii. further extensions of gaussian—type basis sets for use in molecular orbital studies of organic molecules. *The Journal of Chemical Physics*, *56*, 2257–2261. doi:10.1063/1.1677527.

Joback, K. G., & Reid, R. C. (1987). Estimation of pure-component properties from group-contributions. *Chemical Engineering Communications*, *57*, 233–243.

Kendall, R. A., Dunning Jr, T. H., & Harrison, R. J. (1992). Electron affinities of the first-row atoms revisited. systematic basis sets and wave functions. *The Journal of chemical physics*, *96*, 6796–6806.

Kumar, A., Neese, F., & Valeev, E. F. (2020). Explicitly correlated coupled cluster method for accurate treatment of open-shell molecules with hundreds of atoms. *The Journal of chemical physics*, *153*, 094105.

Kurtén, T., Møller, K. H., Nguyen, T. B., Schwantes, R. H., Misztal, P. K., Su, L., Wennberg, P. O., Fry, J. L., & Kjaergaard, H. G. (2017). Alkoxy radical bond scissions explain the anomalously low secondary organic aerosol and organonitrate yields from α-pinene+ no3. *The Journal of Physical Chemistry Letters*, *8*, 2826–2834.

Lee, C., Yang, W., & Parr, R. G. (1988). Development of the colle-salvetti correlation-energy formula into a functional of the electron density. *Physical review B*, *37*, 785.

Møller, K. H., Otkjær, R. V., Hyttinen, N., Kurtén, T., & Kjaergaard, H. G. (2016). Cost-effective implementation of multiconformer transition state theory for peroxy radical hydrogen shift reactions. *The Journal of Physical Chemistry A*, *120*, 10072–10087.

Myhre, G., Shindell, D., Bréon, F., Collins, W., Fuglestvedt, J., Huang, J., Koch, D., Lamarque, J., Lee, D., Mendoza, B. et al. (2013). Climate change 2013: the physical science basis. *Contribution of working group I to the fifth assessment report of the intergovernmental panel on climate change*, *6*.

NBO 7.0 (2018). *Natural Bond Orbital*. E. D. Glendening, J. K. Badenhoop, A. E. Reed, J. E. Carpenter, J. A. Bohmann, C. M. Morales, P. Karafiloglou, C. R. Landis, and F. Weinhold, Theoretical Chemistry Institute, University of Wisconsin Madison, WI.

Neese, F. (2012). The orca program system. *Wiley Interdiscip. Rev. Comput. Mol. Sci.*, *2*, 73–78. URL: `http://dx.doi.org/10.1002/wcms.81`. doi:`10.1002/wcms.81`.

Neese, F. (2018). Software update: the orca program system, version 4.0. *Wiley Interdisciplinary Reviews: Computational Molecular Science*, *8*, e1327.

Ng, N. L., Brown, S. S., Archibald, A. T., Atlas, E., Cohen, R. C., Crowley, J. N., Day, D. A., Donahue, N. M., Fry, J. L., Fuchs, H. et al. (2017). Nitrate radicals and biogenic volatile organic compounds: oxidation, mecha-

nisms, and organic aerosol. *Atmospheric chemistry and physics*, *17*, 2103–2162.

Park, J., Jongsma, C. G., Zhang, R., & North, S. W. (2004). Oh/od initiated oxidation of isoprene in the presence of o2 and no. *The Journal of Physical Chemistry A*, *108*, 10688–10697.

Peterson, K. A., Adler, T. B., & Werner, H.-J. (2008). Systematically convergent basis sets for explicitly correlated wavefunctions: The atoms h, he, b–ne, and al–ar. *The Journal of chemical physics*, *128*, 084102. doi:10.1063/1.2831537.

Pope III, C. A., & Dockery, D. W. (2006). Health effects of fine particulate air pollution: lines that connect. *Journal of the air & waste management association*, *56*, 709–742.

Pye, H. O., Luecken, D. J., Xu, L., Boyd, C. M., Ng, N. L., Baker, K. R., Ayres, B. R., Bash, J. O., Baumann, K., Carter, W. P. et al. (2015). Modeling the current and future roles of particulate organic nitrates in the southeastern united states. *Environmental Science & Technology*, *49*, 14195–14203.

Reed, A. E., Curtiss, L. A., & Weinhold, F. (1988). Intermolecular interactions from a natural bond orbital, donor-acceptor viewpoint. *Chemical Reviews*, *88*, 899–926.

Roth, H. D., & Herbertz, T. (1993). The structure of simple vinylcyclopropane radical cations: evidence for conjugation between alkene and cyclopropane groups. *Journal of the American Chemical Society*, *115*, 9804–9805.

Saitow, M., Becker, U., Riplinger, C., Valeev, E. F., & Neese, F. (2017). A new near-linear scaling, efficient and accurate, open-shell domain-based local pair natural orbital coupled cluster singles and doubles theory. *The Journal of chemical physics*, *146*, 164105.

Schraufnagel, D. E. (2020). The health effects of ultrafine particles. *Experimental & molecular medicine*, *52*, 311–317.

Shrivastava, M., Cappa, C. D., Fan, J., Goldstein, A. H., Guenther, A. B., Jimenez, J. L., Kuang, C., Laskin, A., Martin, S. T., Ng, N. L. et al. (2017).

Recent advances in understanding secondary organic aerosol: Implications for global climate forcing. *Reviews of Geophysics*, *55*, 509–559.

Spartan'16 (2016). *Spartan*. Wavefunction, Inc.: Irvine, CA.

Spittler, M., Barnes, I., Bejan, I., Brockmann, K., Benter, T., & Wirtz, K. (2006). Reactions of no3 radicals with limonene and α-pinene: Product and soa formation. *Atmospheric Environment*, *40*, 116–127.

Tee, L. S., Gotoh, S., & Stewart, W. E. (1966). Molecular parameters for normal fluids. lennard-jones 12-6 potential. *Industrial & Engineering Chemistry Fundamentals*, *5*, 356–363.

Thomsen, D., Elm, J., Rosati, B., Skønager, J. T., Bilde, M., & Glasius, M. (2021). Large discrepancy in the formation of secondary organic aerosols from structurally similar monoterpenes. *ACS Earth and Space Chemistry*, *5*, 632–644.

Vereecken, L., & Peeters, J. (2009). Decomposition of substituted alkoxy radicals—part i: a generalized structure–activity relationship for reaction barrier heights. *Physical Chemistry Chemical Physics*, *11*, 9062–9074.

Wängberg, I., Barnes, I., & Becker, K. (1997). Product and mechanistic study of the reaction of no3 radicals with α-pinene. *Environmental science & technology*, *31*, 2130–2135.

Wayne, R. P., Barnes, I., Biggs, P., Burrows, J., Canosa-Mas, C., Hjorth, J., Le Bras, G., Moortgat, G., Perner, D., Poulet, G. et al. (1991). The nitrate radical: Physics, chemistry, and the atmosphere. *Atmospheric Environment. Part A. General Topics*, *25*, 1–203.

Yeh, G. K., Claflin, M. S., & Ziemann, P. J. (2015). Products and mechanism of the reaction of 1-pentadecene with no3 radicals and the effect of a- ono2 group on alkoxy radical decomposition. *The Journal of Physical Chemistry A*, *119*, 10684–10696.

Zádor, J., Martí, C., Van de Vijver, R., Johansen, S. L., Yang, Y., Michelsen, H. A., & Najm, H. N. (2023). Automated reaction kinetics of gas-phase organic species over multiwell potential energy surfaces. *The Journal of Physical Chemistry A*, *127*, 565–588.

Zhang, H., Yee, L. D., Lee, B. H., Curtis, M. P., Worton, D. R., Isaacman-VanWertz, G., Offenberg, J. H., Lewandowski, M., Kleindienst, T. E., Beaver, M. R. et al. (2018). Monoterpenes are the largest source of summertime organic aerosol in the southeastern united states. *Proceedings of the National Academy of Sciences*, *115*, 2038–2043.

Zhang, Q., Jimenez, J. L., Canagaratna, M., Allan, J. D., Coe, H., Ulbrich, I., Alfarra, M., Takami, A., Middlebrook, A., Sun, Y. et al. (2007). Ubiquity and dominance of oxygenated species in organic aerosols in anthropogenically-influenced northern hemisphere midlatitudes. *Geophysical research letters*, *34*.

Zhao, Q., Møller, K. H., Chen, J., & Kjaergaard, H. G. (2022). Cost-effective implementation of multiconformer transition state theory for alkoxy radical unimolecular reactions. *The Journal of Physical Chemistry A*, *126*, 6483–6494.